

UDC 661.657:539.89

**S. Wang** (Las Vegas, NV, USA; Los Alamos, NM, USA; Chengdu, P. R. China)

**X. Yu, J. Zhang** (Los Alamos, NM, USA)

**Y. Zhang, L. Wang** (Las Vegas, NV, USA)

**K. Leinenweber** (Tempe, AZ, USA)

**H. Xu** (Los Alamos, NM, USA)

**D. Popov, Ch. Park** (Argonne, Illinois, USA)

**W. Yang** (Argonne, Illinois, USA; Shanghai, P. R. China)

**D. He** (Chengdu, P. R. China)

**Y. Zhao\*** (Las Vegas, NV, USA; Los Alamos, NM, USA)

\**Yusheng.Zhao@UNLV.edu*

### **Crystal structures, elastic properties, and hardness of high-pressure synthesized CrB<sub>2</sub> and CrB<sub>4</sub>**

*Chromium tetraboride (CrB<sub>4</sub>), a recently proposed candidate for superhard materials, has been synthesized at high pressure and temperature by a solid-state reaction. As a byproduct, chromium diboride (CrB<sub>2</sub>) also forms and co-exists with CrB<sub>4</sub> in the final product. The comparative studies of crystal structure, elastic property, and hardness of both phases have been conducted at the same sample environment conditions. The crystal structure of CrB<sub>4</sub> has been refined with an orthorhombic symmetry of Immm (space group no. 71) or Pnmm (space group no. 58) using X-ray diffraction data. Further simulations indicate that the structural distinction between Immm and Pnmm can be resolved by neutron diffraction, due to the high scattering cross-section of boron (<sup>11</sup>B) by neutrons. Although CrB<sub>2</sub> and CrB<sub>4</sub> have close bulk modulus at about 230 GPa, the measured asymptotic Vickers hardness yields 16 GPa for CrB<sub>2</sub> but 30 GPa for CrB<sub>4</sub>, which is nearly two times that of CrB<sub>2</sub>. The dramatic enhancement in hardness in CrB<sub>4</sub> is attributed to the strong three-dimensional Cr–B network, in contrast to the layered lattice structure of hexagonal CrB<sub>2</sub>.*

**Keywords:** Chromium borides, CrB<sub>4</sub>, CrB<sub>2</sub>, high-pressure synthesis, structure, compressibility, superhard material.

#### **INTRODUCTION**

Incorporation of small, light, and covalent elements, such as B, C, and N, into the crystalline lattices of large, electron-rich transition metals (e.g., W and Re) holds the promise to produce a new class of super- or ultra-hard materials that are more cost-effective and versatile than traditional superhard materials of diamond and cBN [1–6]. Since 2007, inspired by frontier research on ReB<sub>2</sub> by Chung et al. [7], there has been a new surge of research interest in searching for ultra-incompressible and superhard transition-metal (TM) borides, nitrides, and carbides. These efforts have led to a series of new system including diborides (ReB<sub>2</sub> [8–10] and RuB<sub>2</sub> [10]), tetraborides (WB<sub>4</sub> [11, 12], FeB<sub>4</sub> [13], MnB<sub>4</sub> [14, 15], and CrB<sub>4</sub> [16–18]), nitrides (Re<sub>x</sub>N [19] and WN<sub>x</sub> [20]), and carbides (Re<sub>2</sub>C [21]).

© S. WANG, X. YU, J. ZHANG, Y. ZHANG, L. WANG, K. LEINENWEBER, D. POPOV, CH. PARK, W. YANG, D. HE, Y. ZHAO, 2014

Among them TM tetraborides ( $\text{TMB}_4$ ) are of particular interest because they often exhibit superior hardness over their diboride, nitride, and carbide counterparts, primarily due to their high boron content and associated three-dimensional (3D) covalent network [22].

Because of the experimental difficulties associated with the synthesis of phase-pure TM borides, the crystal structure and intrinsic hardness of  $\text{TMB}_4$  continue to be a subject of debate [23, 24]. However, increasing experimental evidence indicates that hexagonal  $\text{WB}_4$ , the hardest TM boride known to date, has an asymptotic (i.e., load-independent) Vickers hardness of  $H_V \approx 30$  GPa [10–12], which is close to those of pure  $\gamma$ -boron ( $\sim 30$  GPa) and  $\beta$ -boron ( $\sim 26$  GPa) but not in that superhard regime [25]. In addition, due to their layered stacking along the  $c$ -axis of alternating TM layers and B dimers, hexagonal TM tetraborides are structurally unfavorable to form mechanically isotropic superhard materials [22]. A similar atomic stacking configuration also occurs in most TM diborides with hexagonal crystal symmetries, for examples,  $P6/mmm$  (S.G. no. 191) in  $\text{TiB}_2$  and  $P6_3/mmc$  (S.G. no. 194) in  $\text{ReB}_2$  [1, 6]. As pointed out by Wang et al. [22], the hardness of hexagonal  $\text{TMB}_4$  is predominantly determined by the covalently B–B bonded network between the intercalated boron dimers in the parent lattice of transition metals. From this point of view, the primary role that TM lattice plays is a “place-holder” for boron dimers, which limits the hardness of hexagonal  $\text{TMB}_x$  to the level of elemental boron and boron-rich compounds with asymptotic  $H_V \approx 26$ –30 GPa [25, 26]. However, after an exhausting search of the known structures for  $\text{TMB}_x$ , the orthorhombic  $\text{TMB}_4$  (TM = Cr, Mn, and Fe) is found to exhibit a 3D bonding network between TM and boron [15, 17, 27], which is structurally more favorable than hexagonal  $\text{TMB}_4$  for producing mechanically isotropic borides. As expected, recent reports show that the orthorhombic  $\text{FeB}_4$  and  $\text{MnB}_4$  possess a superior nanoindentation hardness of 62 GPa and a Vickers hardness of  $H_V = 37.4$  GPa under a load of 9.8 g [13, 14], approaching the superhard regime as defined by the asymptotic  $H_V \geq 40$  GPa. Strikingly, both borides also exhibit intriguing superconducting and magnetic properties [13, 14, 16].

Chromium tetraboride,  $\text{CrB}_4$ , was first synthesized in 1962 [27] and has recently been reemerged as a promising candidate for achieving superhardness [16–18]. However, the synthesis of single-phase  $\text{CrB}_4$  is still challenging because  $\text{CrB}_2$  often co-exists as a secondary phase in the final product, indicating that  $\text{CrB}_2$  is thermodynamically more stable in the Cr–B system [17, 18]. In addition, the detailed structure of  $\text{CrB}_4$  is an unsettled issue between orthorhombic symmetries of  $Immm$  and  $Pnmm$  [17]. A similar structure controversy has also been reported in  $\text{MnB}_4$  [14, 28]. In this work, for the first time, we synthesized  $\text{CrB}_4$  through a solid-state reaction between chromium and boron under high-pressure ( $p$ )/high-temperature ( $T$ ) conditions. The final product was characterized by powder X-ray diffraction (XRD), high- $p$  diamond-anvil cell (DAC) compression experiments, and Vickers hardness measurements.

## EXPERIMENTAL

Commercially available chemical pure Cr (> 99.9% purity) and B (> 99.9% purity) powders in a molar ratio Cr : B = 1 : 4.5 were homogeneously mixed for the synthesis of  $\text{CrB}_4$ . Excessive boron was used to eliminate the possible  $\text{CrB}_2$  byproduct. High  $p$ ,  $T$  synthetic experiments were carried out in a multianvil cubic press at the Arizona State University, USA. Pressure and temperature generation and calibration were described previously [29]. A prepressed pellet of the starting mixture was placed in a hexagonal boron nitride (hBN) capsule, which served as a

high-pressure sample chamber and was surrounded by a graphite heater for in situ high temperature. Experimental details are described elsewhere [29].

The final product was characterized by powder X-ray diffraction with copper target. The crystal structures of borides were refined using the Rietveld method with the GSAS software [30]. The Vickers hardness was measured using a Micromet–2103 hardness tester on the well-sintered bulk sample at 25–1000 g loading force and a 15 s dwelling time.

High pressure synchrotron X-ray diffraction (XRD) experiments using the diamond-anvil cell (DAC) were performed at the HPCAT 16BM–D beamline of the Advance Photon Source (APS), Argonne National Laboratory. The boride powder was loaded into the sample hole in a stainless steel gasket pre-indented to 30 micron thick with neon as the pressure-transmitting medium. A few ruby balls were also loaded in the same sample chamber to serve as the internal pressure standard [31]. The sample was compressed up to 20 GPa at room temperature. The two-dimensional angle-dispersive XRD patterns were collected with focused monochromatic X-rays with wavelength 0.41325 Å and a Mar3450 imaging plate. The program Fit2D was used to integrate all 2D images into one-dimensional diffraction profiles [32].

## RESULTS AND DISCUSSION

Figure 1, *a* shows the XRD pattern of the experimental run product synthesized at 14 GPa and 1200 °C for 45 min. CrB<sub>4</sub> and CrB<sub>2</sub> are identified as major phases in the recovered sample at ~ 45% and ~ 50% mole fractions, respectively. About 5% hBN originated from BN sample container is also detected. Even though a 12.5% excess of boron was used in the starting material to prepare CrB<sub>4</sub>, CrB<sub>2</sub> still formed as a major byproduct under the present experimental conditions. However, the unreacted boron left behind in the final product cannot be detected by X-ray diffraction (see Fig. 1, *a*), indicating an amorphous state. The similar phenomenon has also been found previously in the synthesis of ReB<sub>2</sub> and WB<sub>4</sub> [9, 11]. For synthesis at atmospheric pressure, recent studies show that a prolonged heating duration of 8–14 days can increase the phase fraction of CrB<sub>4</sub> to as high as 90% [17, 18], indicating that CrB<sub>2</sub> may be an intermediate phase formed in advance of CrB<sub>4</sub>. Obviously, the formation of CrB<sub>4</sub> is kinetically sluggish at atmospheric pressure. Although the heating time is short in our high-*p* synthesis (i.e., only 45 min), the obtained CrB<sub>4</sub> has a moderate fraction of 45% in the recovered sample, indicating that the formation of CrB<sub>4</sub> is kinetically more favorable at high pressure. However, our later synthesis shows that CrB<sub>4</sub> does not form at all at a lower pressure of 8 GPa and temperature of 1200 °C for 1 hour, which is similar to the case of FeB<sub>4</sub> with reported formation pressures of 8–18 GPa [13]. But for MnB<sub>4</sub>, it can be synthesized at a lower pressure of 3 GPa [14].

As shown in Fig. 1, *a*, the refined structure of CrB<sub>2</sub> is hexagonal with space group *P6/mmm* (no. 191), a symmetry typical for many metal diborides [1]. The refined lattice parameters are  $a = 2.9747(2)$  Å and  $c = 3.0660(2)$  Å, which agree well with the reported values [16–18]. The details of the refined structural parameters are summarized in the table. A subset of Bragg peaks in Fig. 1, *a* can be indexed in terms of orthorhombic phase, which belongs to crystalline CrB<sub>4</sub>. The structural refinements were thus performed using an earlier proposed symmetry of *Immm* (no. 71). The obtained lattice parameters are  $a = 4.7481(1)$  Å,  $b = 5.4815(3)$  Å, and  $c = 2.8662(2)$  Å (see the table for details), which is consistent with the recent studies [16–18]. The corresponding structures of CrB<sub>2</sub> and CrB<sub>4</sub> are shown in Figs. 1, *b* and *c* in polyhedral views. Evidently, the Cr and B ions in CrB<sub>4</sub> are

covalently bonded to form a strong 3D network, similar to that in  $\text{MnB}_4$  [28]. In contrast, the Cr–B bonds in  $\text{CrB}_2$  are two-dimensional from the layer-structured stacking sequence, which leads to lower hardness as discussed below. Based on electron diffraction measurements, a new space group,  $Pnmm$  (no. 58), has recently been proposed for  $\text{CrB}_4$  [17], which is selected in this work as the structural candidate for refinement. However, within the resolution of our XRD data, the refined results using  $Pnmm$  are indistinguishable from those using  $Immm$ , as reflected by the similar refinement agreement indices (see the table).

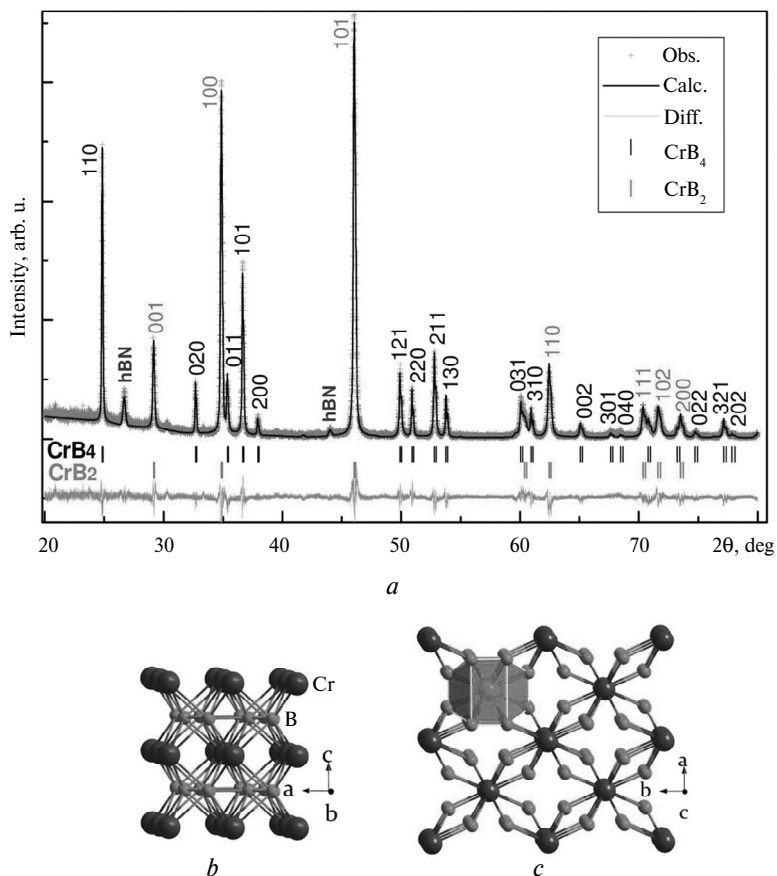


Fig. 1. (a) Rietveld analysis of powder X-ray diffraction pattern of co-existing  $\text{CrB}_2$  and  $\text{CrB}_4$  phases. The sample was synthesized at 14 GPa and 1200 °C for 45 min. Crosses and black lines represent the observed and calculated profiles, respectively. The difference curve between the observed and calculated profiles is shown in light gray. The peak positions of Bragg reflections for  $\text{CrB}_4$  and  $\text{CrB}_2$  are tick marked. Impurity phase hBN originates from the capsule material used for high pressure synthesis. (b) Polyhedral view of the structures of  $\text{CrB}_2$  (left,  $2 \times 2 \times 2$  unit cell) and  $\text{CrB}_4$  (right,  $2 \times 2 \times 2$  unit cell (c)).

To better illustrate the distinction between the two space groups of  $\text{CrB}_4$ , the powder X-ray and neutron diffraction patterns are simulated for  $Pnmm$  and  $Immm$ , which are shown in Figs. 2, a and b. The corresponding structures are depicted in Figs. 2, b and c. Evidently, a major difference between the two structures is the atomic positions of boron with the lower-symmetry  $Pnmm$  structure having tilted  $[\text{CrB}_{12}]$  coordination (see Figs. 2, c and d). Since boron is a light element and has a small X-ray scattering factor, the structural distinction between  $Pnmm$  and  $Immm$

cannot be resolved by X-ray diffraction due to the small scattering cross-section of boron atoms. By contrast, the neutron scattering cross-section of an element does not scale with its atomic number, and neutrons are more sensitive to the presence of light elements (e.g., boron) in a crystal structure. As illustrated in Fig. 2, *b*, the *Pnmm* and *Immm* structures can be readily distinguished by neutron diffraction (NPD), because some additional peaks for the low-symmetry structure *Pnmm* phase that are hard to discern in its XRD pattern are much stronger in the neutron pattern. Hence, further neutron diffraction measurement on  $\text{Cr}^{11}\text{B}_4$  is warranted to resolve the structural controversy.

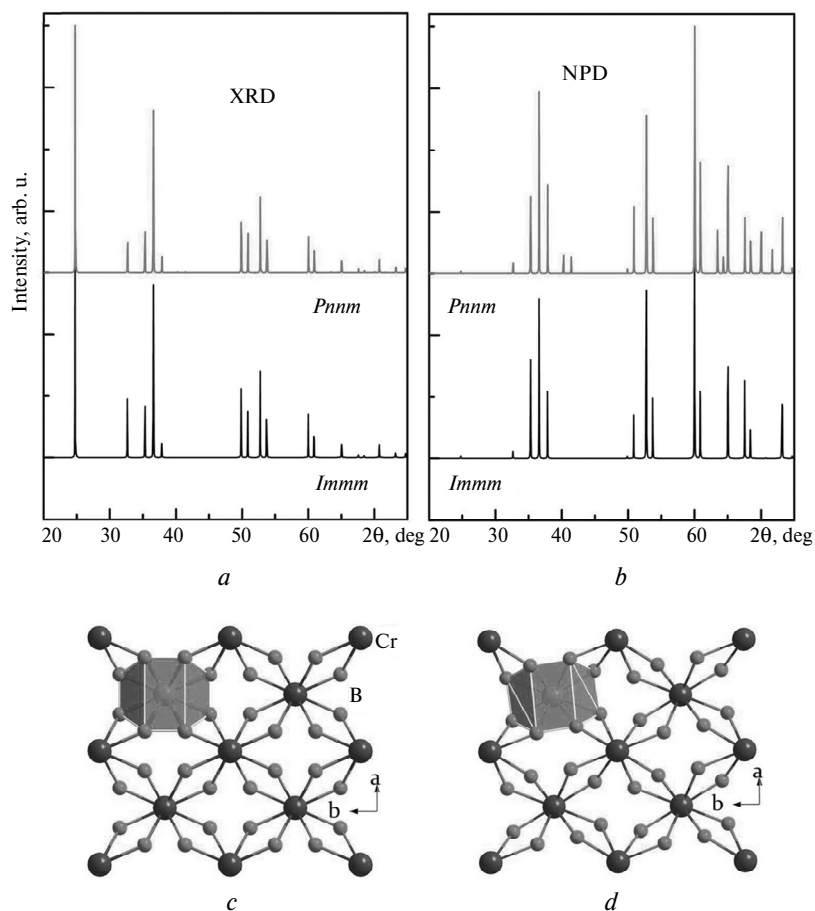


Fig. 2. (a) Simulated powder X-ray (left panel) and (b) neutron (right panel) diffraction patterns for  $\text{CrB}_4$  based on two possible structures of *Immm* (no. 71) and *Pnmm* (no. 58). (c) Crystal structures of *Immm* and *Pnmm* (d) (see the table for structure details).

### Summary of the refined structural parameters for $\text{CrB}_2$ and $\text{CrB}_4$

	$\text{CrB}_2$	$\text{CrB}_4$	
<i>p, T</i> conditions		Ambient conditions	
Space group	<i>P6/mmm</i> (no. 191)	<i>Immm</i> (no. 71)	<i>Pnmm</i> (no. 58)
Cell content	$\text{CrB}_2$	$\text{Cr}_2\text{B}_8$	$\text{Cr}_2\text{B}_8$
$a_0, b_0, c_0, \text{\AA}$	2.9747(2), 2.9747(2), 3.0660(2)	4.7481(1), 5.4815(3), 2.8662(2)	4.7483(2), 5.4817(3), 2.8663(2)

Contd.

Cell volume, Å <sup>3</sup>	23.501	74.584	74.585
$\rho$ , g·cm <sup>-3</sup>	5.202	4.241	4.241
Cr positions	1a, (0, 0, 0)	2a, (0, 0, 0)	2c, (0, 0, 0)
B positions	2d, (1/3, 2/3, 1/2)	8n, (0.191, 0.350, 0)	4g, (0.1640, 0.6351, 0) 4g, (0.2236, 0.3210, 0)
$R_{wp}$ , % $R_p$ , % $\chi^2$	8.6, 6.2, 4.1		8.4, 6.3, 4.0

Phase stability and compressibility of CrB<sub>4</sub> were investigated by synchrotron X-ray diffraction in a diamond-anvil cell (DAC). Figure 3 shows the selected XRD patterns collected under room-temperature compression. Because both CrB<sub>4</sub> and CrB<sub>2</sub> exist in the sample, it allows us to conduct a comparative study of the two phases with exactly the same sample environments. The results show that CrB<sub>2</sub> and CrB<sub>4</sub> are structurally stable up to 25 GPa, and no phase transition was observed. The derived pressure–volume data for CrB<sub>2</sub> and CrB<sub>4</sub> are fitted to the second order Birch–Murnaghan equation of state [33], as shown in Fig. 4. The obtained bulk moduli,  $B_0$ , for CrB<sub>2</sub> and CrB<sub>4</sub> are 228(5) GPa and 232(6) GPa, respectively, which agree well with the results of first–principles calculations [28, 34]. The obtained bulk moduli are close to the boron-rich compounds, such as B<sub>13</sub>N<sub>2</sub> [35], B<sub>6</sub>O [36], and B<sub>4</sub>C [37]. In spite of the fact that CrB<sub>2</sub> and CrB<sub>4</sub> have a nearly identical bulk modulus, they show different behaviors in the axial compressibility as illustrated in Fig. 5. For CrB<sub>2</sub>, the *c*-axis is significantly more compressible than the *a*-axis (see Fig. 5, *a*), which is consistent with its layered atomic stacking along *c*-axis

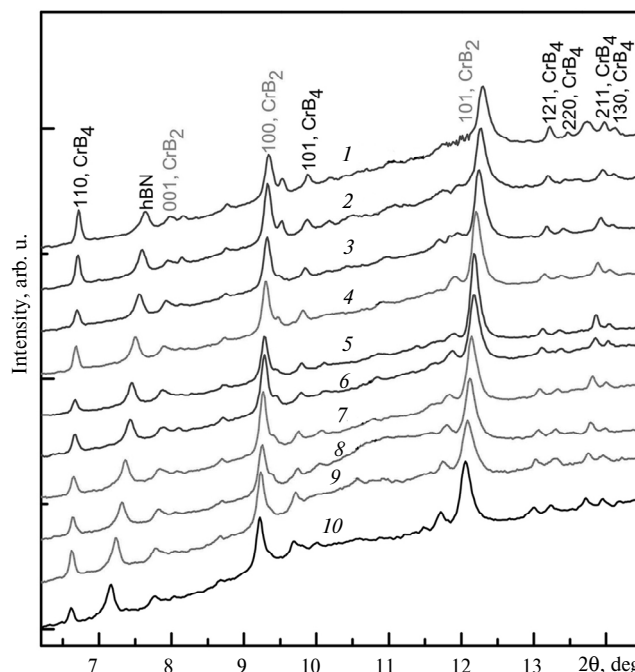


Fig. 3. Selected high-pressure synchrotron X-ray diffraction patterns collected at room temperature in a diamond–anvil cell: 15.7 (1), 13.6 (2), 12.0 (3), 10.2 (4), 8.9 (5), 7.7 (6), 5.8 (7), 4.5 (8), 2.8 (9), 1.4 (10). The incident X-ray wavelength is  $\lambda = 0.41326$  Å.

(see Fig. 1, *b*). For CrB<sub>4</sub>, as shown in Fig. 5, *b*, the compression along the three crystallographic axes is more isotropic than in CrB<sub>2</sub>. Interestingly, the *b*-axis is the least compressible although it has the largest lattice parameter (5.481 Å), whereas the most compressible axis, the *c* axis, corresponds to the shortest lattice parameter (*c* = 2.866 Å), which are in agreement with the recent results of first-principles simulations [28]. This anomalous compressive behavior has only sparsely been reported [20], and is likely to be associated with the peculiar atomic arrangements in orthorhombic CrB<sub>4</sub>.

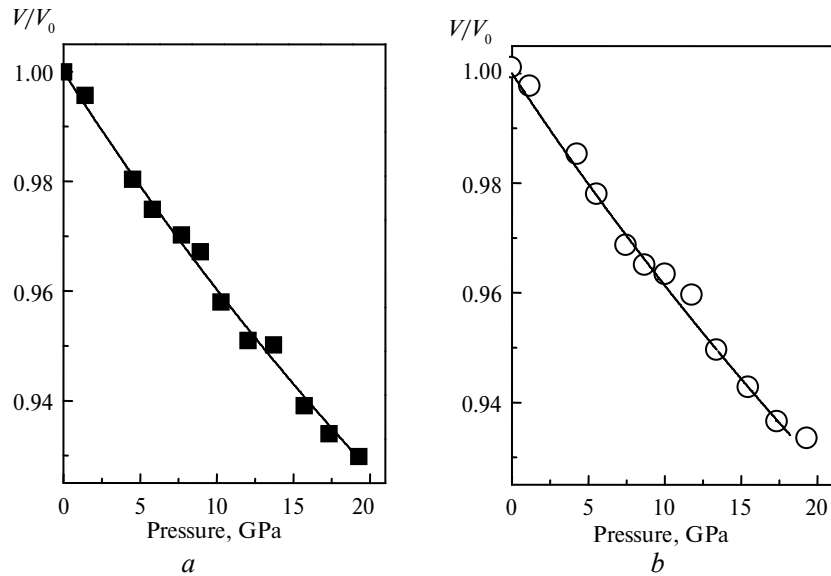


Fig. 4. Volume–pressure data fitted to the second order Birch–Murnaghan equation of state for (a) CrB<sub>2</sub> and (b) CrB<sub>4</sub>.

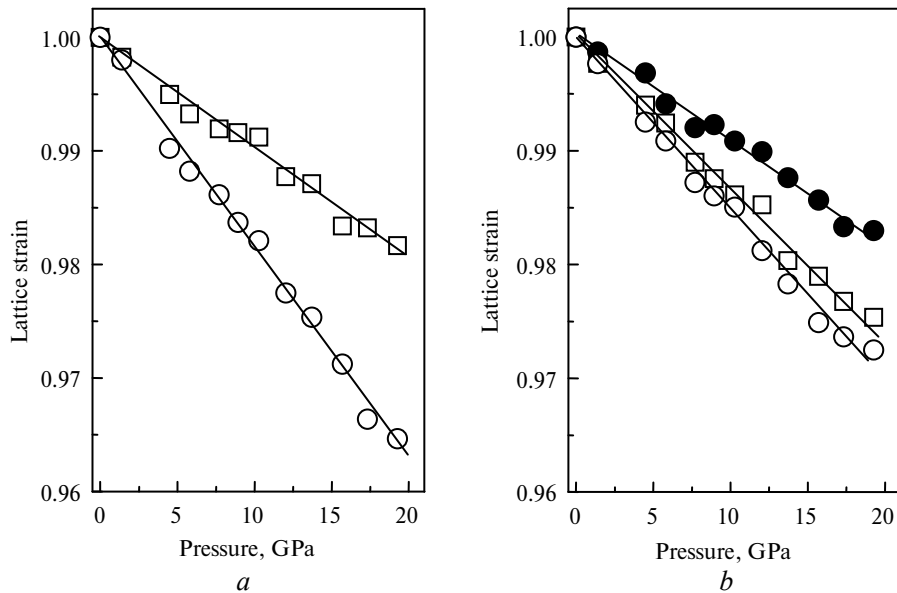


Fig. 5. Relative cell parameters as a function of pressure for (a) CrB<sub>2</sub> and (b) CrB<sub>4</sub> derived from high-pressure X-ray diffraction data.

Vickers hardness measurements were performed on the recovered bulk sample with mixed phases of  $\text{CrB}_2$  and  $\text{CrB}_4$ . Figure 6 shows a typical fluorescence image from the polished sample surface, which was taken using the microscopy system of the hardness tester with a magnification of  $\times 400$ . Clearly,  $\text{CrB}_4$  and  $\text{CrB}_2$  are distinguishable by dark and bright regions, respectively, allowing their indentation measurements to be conducted on each of the two boride phases. As shown in Fig. 7, the determined asymptotic hardness of  $\text{CrB}_4$  is  $\sim 30$  GPa, which is close to that of the known hardest  $\text{WB}_4$  and is presumably attributed to its strong 3D Cr–B bonding network. However, the layer-structured  $\text{CrB}_2$  has a substantially lower hardness of  $\sim 16$  GPa, which agrees with the previously reported value [3].

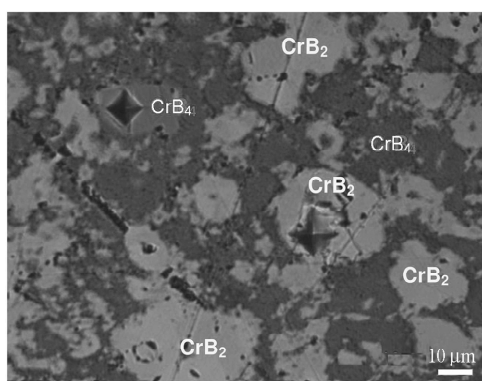


Fig. 6. A fluorescence image of the indentations produced at an indenter tip load of 200 g with a dwell time of 15 s. The dark and bright regions are  $\text{CrB}_4$  and  $\text{CrB}_2$ , respectively.

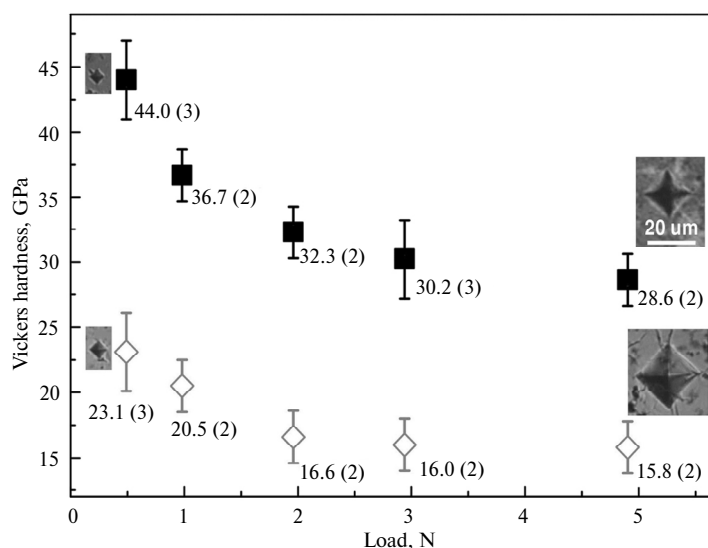


Fig. 7. Vickers hardness of  $\text{CrB}_4$  (solid squares) and  $\text{CrB}_2$  (open diamonds) as a function of indenter tip load. Insets are the selected images of indentation.

## CONCLUSIONS

In summary, for the first time, we synthesized the orthorhombic  $\text{CrB}_4$  phase at high  $p$ ,  $T$  conditions at 14 GPa and 1200 °C through a solid-state reaction between chromium and boron elements. The only byproduct is  $\text{CrB}_2$ , which may be an intermediate phase prior to the formation of  $\text{CrB}_4$ . Despite a short heating time of 45 minutes in the high- $p$  synthesis, the phase mole fraction of  $\text{CrB}_4$  in the final



product yields a high fraction value of 45%, indicating accelerated formation kinetics of CrB<sub>4</sub> at high  $p$ ,  $T$  condition. The refined crystal structures of CrB<sub>2</sub> and CrB<sub>4</sub> are hexagonal  $P6/mmm$  and orthorhombic  $Immm$  or  $Pnmm$ , respectively. Our simulations indicate that the major structural difference between  $Immm$  and  $Pnmm$  is the atomic positions of boron rendering neutron diffraction a more effective approach to resolve these two structures. Based on high- $p$  synchrotron XRD experiment, the obtained bulk moduli of CrB<sub>2</sub> and CrB<sub>4</sub> are 228 GPa and 232 GPa, respectively. Despite the similar bulk moduli, CrB<sub>4</sub> has a much higher asymptotic Vickers hardness of  $\sim 30$  GPa than that of CrB<sub>2</sub> ( $\sim 16$  GPa), which is presumably attributed to the strong three-dimensional Cr–B network in CrB<sub>4</sub>.

Portions of this work were performed at HPCAT, Advanced Photon Source (APS), Argonne National Laboratory. HPCAT operations are supported by DOE–NNSA under Award No. DE-NA0001974 and DOE–BES under Award No. DE-FG02-99ER45775, with partial instrumentation funding by NSF. APS is supported by DOE–BES, under Contract No. DE-AC02-06CH11357. This work is also supported by UNLV High Pressure Science and Engineering Center (HiPSEC), which is a DOE NNSA Center of Excellence operated under Cooperative Agreement DE-FC52-06NA27684, and UNLV start-up funding to Y. Zhao. This research is partially supported by Los Alamos National Laboratory, which is operated by Los Alamos National Security LLC under DOE Contract DE-AC52-06NA25396. HPSynC is supported as part of EFree, an Energy Frontier Research Center funded by DOE–BES under Grant DE-SC0001057.

*Тетраборид хрому (CrB<sub>4</sub>), недавно запропонований як перспективний надтвердий матеріал, був синтезований при високому тиску і температурі шляхом твердофазної реакції. Як побічний продукт, утворюється також диборид хрому (CrB<sub>2</sub>) і співіснує з CrB<sub>4</sub> в кінцевому продукті. Проведено порівняльне вивчення кристалічної структури, пружних властивостей і твердості обох фаз при однакових умовах навколишнього середовища. З використанням даних дифракції рентгенівських променів кристалічна структура CrB<sub>4</sub> визначена як та, що має орторомбічну симетрію  $Immm$  (просторова група № 71) або  $Pnmm$  (просторова група № 58). Подальші модельні експерименти показують, що структурну відмінність між  $Immm$  і  $Pnmm$  можна визначити методом нейтронної дифракції завдяки високому перерізу розсіювання бору (11В) нейтронами. Хоча CrB<sub>2</sub> і CrB<sub>4</sub> мають близький модуль об'ємного стиску  $\sim 230$  ГПа, асимптотично виміряна твердість за Вікерсу дорівнює 16 ГПа для CrB<sub>2</sub>, але 30 ГПа для CrB<sub>4</sub>, що майже в два рази більше, ніж для CrB<sub>2</sub>. Різке підвищення твердості в CrB<sub>4</sub> пов'язують із сильною тривимірною сіткою Cr–B, на відміну від шаруватої структури тратки гексагонального CrB<sub>2</sub>.*

**Ключові слова:** бориди хрому, CrB<sub>4</sub>, CrB<sub>2</sub>, синтез при високому тиску, структура, стисливість, надтвердий матеріал.

*Тетраборид хрому (CrB<sub>4</sub>), недавно предложенный как перспективный сверхтвердый материал, был синтезирован при высоком давлении и температуре путем твердофазной реакции. Как побочный продукт, образуется также диборид хрома (CrB<sub>2</sub>) и сосуществует с CrB<sub>4</sub> в конечном продукте. Проведено сравнительное изучение кристаллической структуры, упругих свойств и твердости обеих фаз при одинаковых условиях окружающей среды. С использованием данных дифракции рентгеновских лучей кристаллическая структура CrB<sub>4</sub> определена как имеющая орторомбическую симметрию  $Immm$  (пространственная группа № 71) или  $Pnmm$  (пространственная группа № 58). Дальнейшие модельные эксперименты показывают, что структурное различие между  $Immm$  и  $Pnmm$  может быть можно определить методом нейтронной дифракции благодаря высокому сечению рассеяния бора (11В) нейтронами. Хотя CrB<sub>2</sub> и CrB<sub>4</sub> имеют близкий модуль объемного сжатия  $\sim 230$  ГПа, асимптотически измеренная твердость по Викерсу равна 16 ГПа для CrB<sub>2</sub>, но 30 ГПа для CrB<sub>4</sub>, что почти в два раза больше, чем для CrB<sub>2</sub>. Резкое повышение твердости в CrB<sub>4</sub> связывают с сильной трехмерной сеткой Cr–B, в отличие от слоистой структуры решетки гексагонального CrB<sub>2</sub>.*

**Ключевые слова:** бориды хрома, CrB<sub>4</sub>, CrB<sub>2</sub>, синтез при высоком давлении, структура, сжимаемость, сверхтвердый материал.

1. *Ivanovskii A. L.* The search for novel superhard and incompressible materials on the basis of higher borides of *s, p, d* metals // *J. Superhard Mater.* – 2011. – **33**, N 2. – P. 73–87.
2. *Veprek S., Zhang R. F., Argon A. S.* Mechanical properties and hardness of boron and boron-rich solids // *Ibid.* – 2011. – **33**, N 6. – P. 409–420.
3. *Zachary Z.* New superhard ternary borides in composite materials // *Metal, Ceramic and Polymeric Composites for Various Uses / Ed. J. Cuppoletti.* – Rijeka, Croatia: InTech, 2011. – P. 61–78.
4. *Brazhkin V. V., Lyapin A. G., Hemley R. J.* Harder than diamond: dreams and reality // *Phil. Mag. A.* – 2002. – **82**, N 2. – P. 231–253.
5. *Brazhkin V., Dubrovinskaia N., Nicol M. et al.* From our readers: What does ‘harder than diamond’ mean? // *Nature Mater.* – 2004. – **3**, N 9. – P. 576–577.
6. *Pierson H. O.* Handbook of refractory carbides and nitrides: properties, characteristics, processing, and applications. – Westwood, NY: Noyes Publications, 1996.
7. *Chung H.-Y., Weinberger M. B., Levine J. B. et al.* Synthesis of ultra-incompressible superhard rhenium diboride at ambient pressure // *Science.* – 2007. – **316**, N 5823. – P. 436–439.
8. *Dubrovinskaia N., Dubrovinsky L., Solozhenko V. L.* Comment on “Synthesis of ultra-incompressible superhard rhenium diboride at ambient pressure” // *Ibid.* – 2007. – **318**, N 5856. – P. 1550.
9. *Qin J., He D., Wang J., Fang L. et al.* Is rhenium diboride a superhard material? // *Adv. Mater.* – 2008. – **20**, N 24. – P. 4780–4783.
10. *Gu Q., Krauss G., Steurer W.* Transition metal borides: superhard versus ultra-incompressible // *Ibid.* – 2008. – **20**, N 19. – P. 3620–3626.
11. *Mohammadi R., Lech A. T., Xie M. et al.* Tungsten tetraboride, an inexpensive superhard material, *Proc. Nat. Acad. Sci.* – 2011. – **108**, N 27. – P. 10958–10962.
12. *Mohammadi R., Xie M., Lech A. T. et al.* Toward inexpensive superhard materials: tungsten tetraboride-based solid solutions // *J. Am. Chem. Soc.* – 2012. – **134**, N 51. – P. 20660–20668.
13. *Gou H., Dubrovinskaia N., Bykova E. et al.* Discovery of a superhard iron tetraboride superconductor // *Phys. Rev. Lett.* – 2013. – **111**, N 15, art. 157002.
14. *Gou H., Tsirlin A. A., Bykova E. et al.* Peierls distortion, magnetism, and high hardness of manganese tetraboride // *Phys. Rev. B.* – 2014. – **89**, art. 064108.
15. *Litterscheid C., Knappschneider A., Albert B.* Single crystal structure of MnB<sub>4</sub> // *Z. Anorg. Allg. Chem.* – 2012. – **638**, N 10. – P. 1608–1608.
16. *Knappschneider A., Litterscheid C., Dzivenko D. et al.* Possible superhardness of CrB<sub>4</sub> // *Inorg. Chem.* – 2013. – **52**, N 2. – P. 540–542.
17. *Niu H., Wang J., Chen X.-Q. et al.* Structure, bonding, and possible superhardness of CrB<sub>4</sub> // *Phys. Rev. B.* – 2012. – **85**, art. 144116.
18. *Knappschneider A., Litterscheid C., Kurzman J. et al.* Crystal structure refinement and bonding patterns of CrB<sub>4</sub>: A boron-rich boride with a framework of tetrahedrally coordinated B atoms // *Inorg. Chem.* – 2011. – **50**, N 21. – P. 10540–10542.
19. *Friedrich A., Winkler B., Bayarjargal L. et al.* Novel rhenium nitrides // *Phys. Rev. Lett.* – 2010. – **105**, art. 085504.
20. *Wang S., Yu X., Lin Z. et al.* Synthesis, crystal structure, and elastic properties of novel tungsten nitrides // *Chem. Mater.* – 2012. – **24**, N 15. – P. 3023–3028.
21. *Zhao Z., Cui L., Wang L. et al.* Bulk Re<sub>2</sub>C: crystal structure, hardness, and ultra-incompressibility // *Cryst. Growth Des.* – 2010. – **10**, N 12. – P. 5024–5026.
22. *Wang M., Li Y., Cui T. et al.* Origin of hardness in WB<sub>4</sub> and its implications for ReB<sub>4</sub>, TaB<sub>4</sub>, MoB<sub>4</sub>, TcB<sub>4</sub>, and OsB<sub>4</sub> // *Appl. Phys. Lett.* – 2008. – **93**, art. 101905.
23. *Zang C., Sun H., Chen C.* Unexpectedly low indentation strength of WB<sub>3</sub> and MoB<sub>3</sub> from First Principles // *Phys. Rev. B.* – 2012. – **86**, art. 180101.
24. *Zhang R. F., Legut D., Lin Z. J. et al.* Stability and strength of transition-metal tetraborides and triborides // *Phys. Rev. Lett.* – 2012. – **108**, art. 255502.
25. *Qin J., Nishiyama N., Ohfuji H. et al.* Polycrystalline  $\gamma$ -boron: as hard as polycrystalline cubic boron nitride // *Scr. Mater.* – 2012. – **67**, N 3. – P. 257–260.
26. *Mukhanov V.A., Kurakevych O. O., Solozhenko V. L.* Thermodynamic model of hardness: particular case of boron-rich solids // *J. Superhard Mater.* – 2010. – **32**, N 3. – P. 167–176.

27. *Andersso S., Lundstro T.* Crystal structure of CrB<sub>4</sub> // *Acta Chem. Scand.* – 1968. – **22**, N 10. – P. 3103–3110.
28. *Yang M., Wang Y., Yao J. et al.* Structural distortion and band gap opening of hard MnB<sub>4</sub> in comparison with CrB<sub>4</sub> and FeB<sub>4</sub> // *J. Solid State Chem.* – 2014. – **213**. – P. 52–56.
29. *Wang W., He D., Wang H. et al.* Research on pressure generation efficiency of 6–8 type multianvil high pressure apparatus // *Acta Phys. Sin.* – 2010. – **59**, N 5. – P. 3107–3115.
30. *Toby B. H.* EXPGUI, a graphical user interface for GSAS // *J. Appl. Cryst.* – 2001. – **34**. – P. 210–213.
31. *Mao H. K., Xu J., Bell P. M.* Calibration of the tuby pressure gauge to 800 kbar under quasi-hydrostatic conditions // *J. Geophys. Res.: Solid Earth.* – 1986. – **91**, N B5. – P. 4673–4676.
32. *Hammersley A. P., Svensson S. O., Hanfland M. et al.* Two-dimensional detector software: from real detector to idealized image or two-theta scan // *High Press. Res.* – 1996. – **14**, N. 4–6. – P. 235–248.
33. *Birch F.* Finite elastic strain of cubic crystals // *Phys. Rev.* – 1947. – **71**, N 11. – P. 809–824.
34. *Okamoto N. L., Kusakari M., Tanaka K. et al.* Anisotropic elastic constants and thermal expansivities in monocrystal CrB<sub>2</sub>, TiB<sub>2</sub>, and ZrB<sub>2</sub> // *Acta Mater.* – 2010. – **58**, N 1. – P. 76–84.
35. *Kurakevych O. O., Solozhenko V. L.* 300-K equation of state of rhombohedral boron subnitride // *Solid State Commun.* – 2009. – **149**, N 47–48. – P. 2169–2171.
36. *Nieto-Sanz D., Loubeyre P., Crichton W., Mezouar M.* X-ray study of the synthesis of boron oxides at high pressure: phase diagram and equation of state // *Phys. Rev. B.* – 2004. – **70**, art. 214108.
37. *Nelmes R. J., Loveday J. S., Wilson R. M. et al.* Observation of inverted-molecular compression in boron carbide // *Phys. Rev. Lett.* – 1995. – **74**, N 12. – P. 2268–2271.

HiPSEC & Physics Department, University of Nevada

Received 15.03.14

LANSCE & EES Divisions, Los Alamos  
National Laboratory

Institute of Atomic & Molecular, Physics,  
Sichuan University

Department of Chemistry and Biochemistry,  
Arizona State University

HPCAT & HPSynC, Geophysical Laboratory,  
Carnegie Institution of Washington

Center for High Pressure Science and Technology  
Advanced Research (HPSTAR), Shanghai, P. R. China